Trauma-Induced Plasmalemma Disruptions in Three-Dimensional Neural Cultures Are Dependent on Strain Modality and Rate

D. Kacy Cullen,[1] Varadraj N. Vernekar,[2] and Michelle C. LaPlaca[2]

Abstract

Traumatic brain injury (TBI) results from cell dysfunction or death following supra-threshold physical loading. Neural plasmalemma compromise has been observed following traumatic neural insults; however, the biomechanical thresholds and time-course of such disruptions remain poorly understood. In order to investigate trauma-induced membrane disruptions, we induced dynamic strain fields (0.50 shear or compressive strain at 1, 10, or $30 \, \sec^{-1}$ strain rate) in 3-D neuronal-astrocytic co-cultures ($> 500 \, \mu m$ thick). Impermeant dyes were present during mechanical loading and entered cells in a strain rate-dependent manner for both shear and compression. Real-time imaging revealed increased membrane permeability in a sub-population of cells immediately upon deformation. Alterations in cell membrane permeability, however, were transient and biphasic over the ensuing hour post-insult, suggesting initial membrane damage and rapid repair, followed by a phase of secondary membrane degradation. At 48 h post-insult, cell death increased significantly in the high-strain-rate group, but not after quasi-static loading, suggesting that cell survival relates to the initial extent of transient structural compromise. Cells were more sensitive to bulk shear deformation than compression with respect to acute permeability changes and subsequent cell survival. These results provide insight into the temporally varying alterations in membrane stability following traumatic loading and provide a basis for elucidating physical cellular tolerances.

Key words: astrocyte; cell mechanics; compression; injury biomechanics; membrane permeability; neuron; neurotrauma, shear; strain rate; 3-D culture; traumatic brain injury

Introduction

Tʀᴀᴜᴍᴀᴛɪᴄ ᴍᴇᴄʜᴀɴɪᴄᴀʟ ʟᴏᴀᴅɪɴɢ to neural cells can lead to devastating consequences. Cells in the brain are not normally subjected to large or rapid deformations due to a unique fluidic and osseous protection system. Supra-threshold physical loading can lead to traumatic brain injury (TBI), the outcomes of which are dependent on the severity of the primary insult and complexity of secondary events (Povlishock and Katz, 2005; Raghupathi, 2004; Saatman et al., 2008). The mechanics associated with brain trauma are variable and complex, but are initiated by impact and/or inertial loading of the head (Gennarelli, 1993; Margulies and Thibault, 1992; Meaney et al., 1995). Typically, supra-threshold loading leads to multi-focal and/or diffuse damage, manifesting in overt lesions, contusions, and disruption of the vasculature

(Gennarelli, 1993; Margulies and Thibault, 1992; Meaney et al., 1995). Collectively, these events may result in significant functional deficits and progressive neural degeneration (Smith et al., 1997; Stein et al., 1993). Currently, there are no effective therapeutic interventions that directly attenuate injury-induced neural cell death (Margulies and Hicks, 2009). Investigation of tissue- and cellular-level injury biomechanics is critically important in refining neural tolerance criteria and developing targeted therapies.

On the cellular level, mechanical loading is a function of complex, three-dimensional (3-D) strain fields consisting of compressive, tensile, and shear strain patterns throughout the brain (Fig. 1A). Based on these biomechanical considerations, as well as heterogeneous brain tissue properties, it is predicted that both shear and compressive deformation are relevant modes of tissue loading in impact (focal/contusion) injuries,

[1]Department of Neurosurgery, Center for Brain Injury and Repair, University of Pennsylvania, Philadelphia, Pennsylvania.
[2]Wallace H. Coulter Department of Biomedical Engineering, Parker H. Petit Institute for Bioengineering and Bioscience, Georgia Institute of Technology, and Emory University, Atlanta, Georgia.
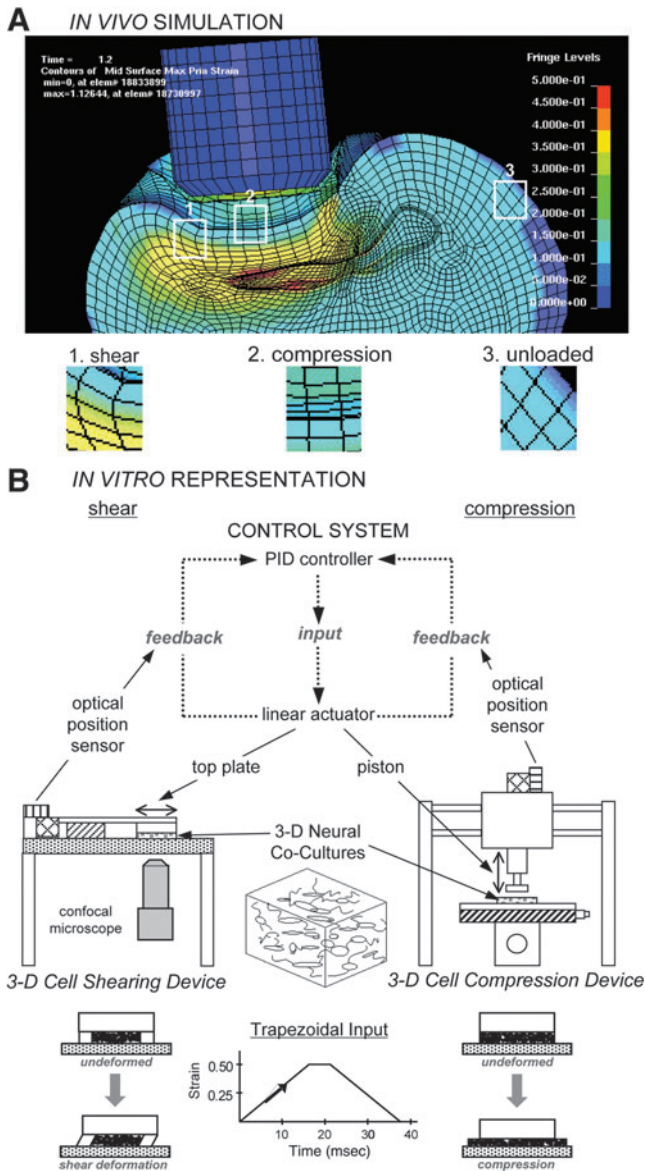
FIG. 1. Finite element analysis (FEA) simulations following traumatic loading *in vivo* and corresponding isolation of tissue bulk loading components *in vitro*. Principal maximum strain profile following controlled cortical impact in a rat as predicted by FEA (**A**). In this example (at t = 1.6 msec), blunt impact results in heterogeneous strain fields, with some regions experiencing shear- or compression-dominated strain fields and some regions left relatively unloaded. Based on these variable and complex tissue responses, we developed custom *in vitro* devices for shear or compressive loading of engineered 3-D tissue surrogates (**B**). Both linear-actuator driven systems impart a prescribed deformation using proportional-integral-derivative (PID) control with positional feedback from optical sensors. While these experimental models produce a particular bulk deformation, local cellular strains will vary based on cellular orientations within the matrix.

whereas shear deformation is predicted to be the dominant mode of tissue loading in inertial (diffuse/acceleration-deceleration) injuries (Holbourne, 1943; LaPlaca et al., 2007; Sahay et al., 1992). The immediate physical consequences of cellular loading may range from complete structural failure,

such as major somatic disruption and axotomy, to more subtle damage, such as axonal stretching, cytoskeletal breakdown, decoupling of sub-cellular structures/organelles, and micro- or nano-tears in the plasmalemma. Physical effects may not directly link to loading conditions, however, since secondary pathophysiology can induce similar structural damage. In particular, acute disruption of the plasmalemma, termed "mechanoporation," may be particularly devastating, as it may trigger disruption of ion homeostasis and exacerbate enzymatic and free radical damage, contributing to subsequent membrane damage in a positive feedback manner (Adibhatla et al., 2006; Farkas et al., 2006).

In the present study, we evaluated alterations in plasmalemma permeability as a function of deformation mode (shear versus compression), loading parameters (strain and strain rate), and time post-insult (milliseconds to hours), in 3-D co-cultures of neurons and astrocytes. We postulate that there is an important link between the physical parameters of traumatic loading and physiological consequences, and furthermore, that shear loading produces more neural damage than compression. Custom-built electromechanical devices enabled controlled and reproducible delivery of a single stimulus to the 3-D cultures; for these studies we used a high shear or compressive strain (0.50) over slow ("quasi-static") or dynamic (≤ 50 msec) durations. Because of the anisotropy and three-dimensionality in these cultures, the resulting strain fields at the cellular level, upon dynamic deformation, are inherently heterogeneous (Cullen and LaPlaca, 2006). Acute membrane compromise was then correlated with longer-term cell death. This experimental design replicates key features of traumatic loading *in vivo*, such as 3-D dynamic loading conditions, multi-cellular composition, and a 3-D distribution of cell-cell/cell-matrix interactions.

Methods

Isolation of primary cortical neurons and cortical astrocytes

All procedures involving animals were approved by the IACUC of the Georgia Institute of Technology. All reagents were from Invitrogen (Carlsbad, CA) unless otherwise noted. Briefly, timed-pregnant Sasco Sprague-Dawley rats (embryonic days 17–18; Charles River, Wilmington, MA) were anesthetized and the uteri were removed. Each fetus was rapidly decapitated and placed in cold calcium- and magnesium-free Hank's balanced salt solution (CMF-HBSS). Cerebral cortices were isolated and dissociated using pre-warmed trypsin (0.25%) + EDTA (1 mM) for 10 min at 37°C, followed by deoxyribonuclease I (DNase I, 0.15 mg/mL; Sigma-Aldrich, St. Louis, MO) in CMF-HBSS. The tissue was triturated with a flame-narrowed Pasteur pipette, centrifuged (1000 rpm for 3 min), and the dissociated cells were resuspended in co-culture medium (Neurobasal medium + 2% B-27 + 1% G-5 + 500 μM L-glutamine).

Astrocytes were isolated from post-natal (days 0–1) Sasco Sprague-Dawley rats. The cortices were isolated, then minced and dissociated following the same process as that described above. Following centrifugation the cell pellets were resuspended in DMEM/F12 + 10% FBS, and transferred to culture flasks. To isolate type I astrocytes, the flasks were mechanically agitated prior to media changes over the first

week in planar culture. As the cells approached $\sim$90% confluence they were re-plated (300 cells/mm^2). Astrocytes were used between passages 4 and 12 to permit phenotypic maturation (Hatten et al., 1991; Liao and Chen, 2001).

Generation of 3-D neuronal-astrocytic co-cultures

Co-cultures were plated in 3-D using separately isolated neurons and astrocytes within Matrigel™ matrix in custom-made culture chambers consisting of a glass cover-slip base and a circular elastomer mold (cross-sectional area 2 cm^2, 1:1 ratio of Sylgard 184 and 186; Dow Corning, Midland, MI). The chambers were pre-treated with 0.05 mg/mL poly-L-lysine (PLL; Sigma-Aldrich) followed by a Matrigel pre-coat (0.5 mL/well at 0.6 mg/mL; Becton Dickinson Biosciences, Bedford, MA) in Neurobasal medium. Matrigel exhibits fluid-like behavior at 4°C (permitting even dispersion of dissociated cells throughout the matrix), and gels at physiological temperature (entrapping cells in 3-D; Kleinman et al., 1986). Co-cultures were plated at 2500 cells/mm^3 at a 1:1 neuron:astrocyte ratio (final Matrigel concentration 7.5 mg/mL) across a thickness of 500–750 μm, and immediately placed at 37°C for gelation, after which 0.5 mL of co-culture medium was added to each culture well. Co-cultures were maintained at 37°C and 5% CO$_2$-95% humidified air, and medium was exchanged at 24 h and every 2 days thereafter. This co-culture system demonstrates robust neurite outgrowth, network formation, neuronal maturation, and high viability (approximately 95%) at 21 days *in vitro* (DIV; Cullen et al., 2011; Irons et al., 2008). Experiments were initiated at 21–23 DIV.

Application of shear or compressive loading

Compressive deformation was applied using a 3-D cell compression device (CCD), and shear deformation was applied using a 3-D cell shearing device (CSD; Cullen and LaPlaca, 2006; Cullen et al., 2007a,2007b; LaPlaca et al., 2005; Fig. 1B). Each device is driven by a linear-actuator (BEI Kimco, San Marcos, CA) coupled to a custom-fabricated digital proportional-integral-derivative controller (25-kHz sampling rate, 16-bit sampling resolution) with closed-loop motion control feedback from an optical position sensor (RGH-34, 400 nm resolution; Renishaw, New Mills, U.K.). Custom code (LabVIEW®; National Instruments, Austin, TX) generated a trapezoidal input of identical strain magnitudes and rates for each device (0.50 strain at a quasi-static strain rate of 1 sec^{-1} or at dynamic strain rates of 10 sec^{-1} or 30 sec^{-1}; loading onset times of 500, 50, and 16.7 msec, respectively). For compression, the linear actuator drives an impactor (piston, diameter 10 mm) compressing the entire culture. For shear deformation, a top plate affixed to a linear actuator delivers lateral motion with respect to the cell chamber to impart simple shear deformation to the entire culture (LaPlaca et al., 2005). Experimental groups consisted of static (unloaded) control cultures or mechanically-loaded cultures. During the static-unloaded control conditions for compression and shear, the cultures were placed into their respective devices, but the devices were not activated. After mechanical deformation or static control conditions, warm medium or buffer with permeability marker (based on the type of assay to be performed) was added and the cultures were returned to the incubator.

Assaying cell permeability

Assaying acute permeability in shear- and compression-deformed cultures. The normally cell-impermeant molecule calcein (623 Da) was used to assess acute alterations in plasmalemma permeability following shear and compressive loading or static conditions ($n = 3$–4 cultures per group). Prior to injury, medium was removed, calcein solution (3.2×10^{-4} M in HBSS) was added, and the cultures were incubated at 37°C for 10 min. Immediately following the insult, cultures were placed at 37°C for 10 min. The cultures were then rinsed with HBSS and immediately imaged using confocal microscopy (LSM 510; Zeiss, Oberkochen, Germany; excitation 495 nm and emission 515 nm). Confocal images were acquired across the full thickness of the cultures and z-stacks were converted to 3-D reconstructions (LSM Image Browser). Cell permeability changes were quantified in at least three regions per culture, with each region defined as having minimum dimensions of $460.7 \times 460.7 \times 100$ μm, and varying systematically based on x, y, and z, to include a range of positions and depths in the culture (with minimal inclusion of edge-containing regions). Calcein$^+$ cells were counted and the density of permeabilized cells per unit volume was calculated.

The fluorescence intensity of randomly selected calcein$^+$ cells from the same cultures was measured to assess the degree of altered permeability. Within each 3-D reconstruction (z-stacks from 3–4 regions per culture, as defined previously), fluorescence intensity line traces were acquired (Fig. 2). An intensity ratio was calculated: (peak intensity – background intensity)/(background intensity). Experimental groups were as follows: shear loading (0.50 strain) at strain rates of 1 sec^{-1} ($n = 5$ cells), 10 sec^{-1} ($n = 44$ cells), 30 sec^{-1} ($n = 51$ cells); and compressive loading (0.50 strain) at strain rates of 1 sec^{-1} ($n = 19$ cells), 10 sec^{-1} ($n = 22$ cells), and 30 sec^{-1} ($n = 75$ cells). The range in the number of cells analyzed per group was due to fewer calcein$^+$ cells per frame following lower strain rate loading.

Assaying acute permeability in real time. Separate 3-D co-cultures were imaged in real time on a confocal microscope during and immediately following shear strain (0.50 shear strain, 10 sec^{-1} or 30 sec^{-1} strain rate) to investigate the temporal pattern of membrane disruptions ($n = 8$ cultures total). Imaging was performed using a $10 \times (921.4 \times 921.4$ μm) or $20 \times (460.7 \times 460.7$ μm) objective. The optical slice thickness was set to establish a suitable signal-to-noise ratio, and ranged from 5–10 μm. Images were captured at a rate of 1–2 frames/sec at a resolution of 256×256 or 512×512 pixels. On a per-cell basis, changes in intracellular fluorescence intensity were measured as a function of time post-insult using LSM Image Browser (Zeiss). Real-time analyses were performed using the 3-D CSD because it was designed to mount on an inverted microscope stage with in-plane translation of the top plate (LaPlaca et al., 2005), permitting tracking of individual cells within the focal plane. Out-of-plane z-axis displacement that is inherent to the compression device does not lend the system to individual cell tracking.

Assaying sub-acute permeability. To assess the sub-acute time course of post-insult alterations in permeability, additional cultures were incubated with calcein solution and/or ethidium homodimer-1 (EthD-1; 4 μM, 857 Da, ex: 495 nm/
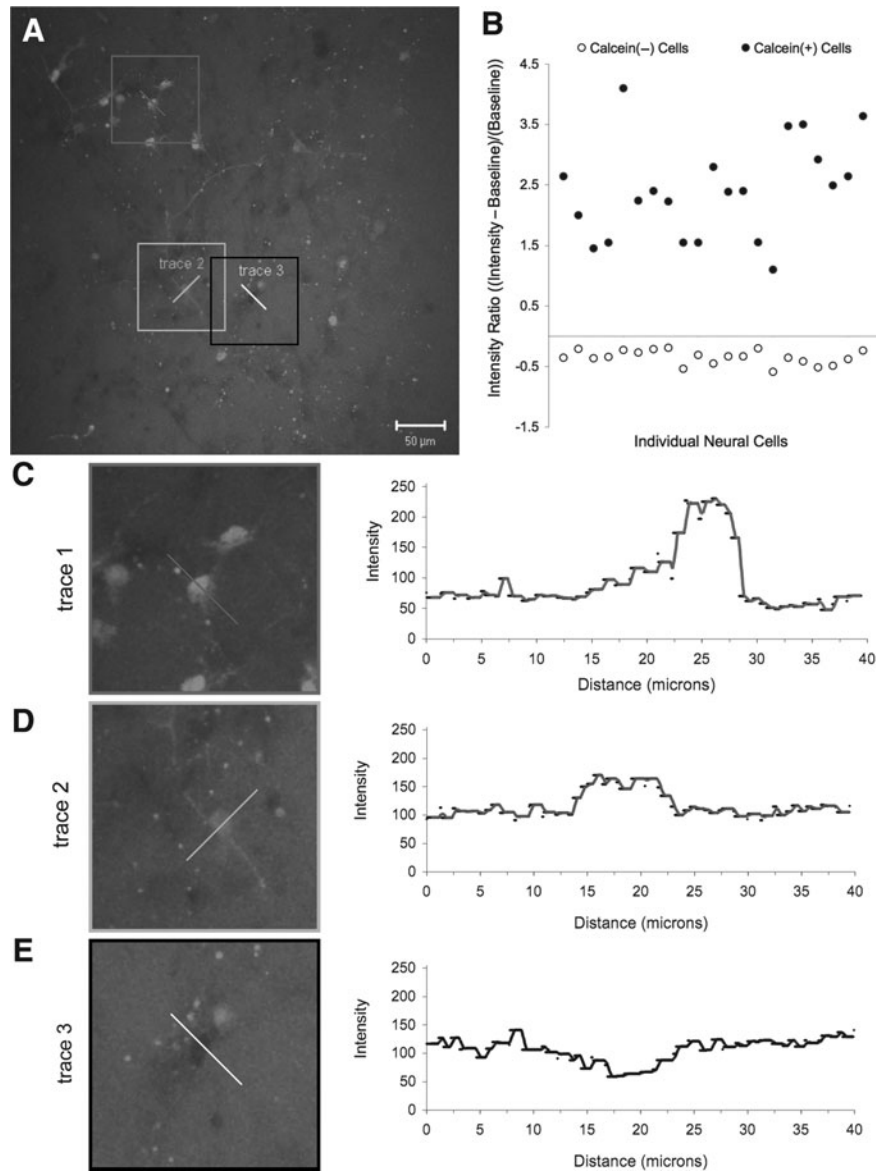
FIG. 2. Methodology employed to quantify the degree of permeability marker uptake. Fluorescence intensity traces, proportional to the amount of calcein uptake, from sample cells in (**A**) are shown in (**C**), (**D**) and (**E**). Cells were classified into two populations (i.e., calcein$^+$ and calcein$^-$) based on fluorescence intensity relative to background (**B**). Cells with a significant calcein uptake exhibited much higher fluorescence relative to background (**C**). Cells with low calcein uptake exhibit a smaller increase in fluorescence relative to background (**D**). Cells that did not take up calcein exhibited lower fluorescence than background (**E**).

em: 635 nm, Molecular Probes, Eugene, OR), before and at various time points up to 60 min following shear deformation (0.50 strain, 10 sec^{-1} strain rate). Specifically, calcein was added prior to loading (0^-) or at 10 min post-insult; EthD-1 was added at 0^-, 10, 60 min, or 6 h post-insult ($n=2$–4 each). Cultures were imaged 10 min following EthD-1 incubation after being rinsed. While both calcein and EthD-1 cross a compromised plasmalemma, EthD-1 irreversibly binds nucleic acids, distinguishing between re-sealed (calcein$^+$ and/or EthD-1$^+$, depending on timing of delivery), and non-resealed (EthD-1$^+$ only) cell populations. Calcein$^+$ cells and EthD-1$^+$ cells were counted from multiple confocal z-stacks per culture (as described above), and the density of calcein$^+$ and EthD-1$^+$

cells per unit volume was calculated (normalized to that of static control cultures).

Assaying permeability by cell type. The subpopulations of neural cells exhibiting permeability changes was evaluated in separate cultures using neurons derived from transgenic mice expressing green fluorescent protein (GFP) cultured with astrocytes (isolated as described above). This permitted neuronal identification, using rhodamine as the permeability marker (3.2×10^{-4} M in HBSS, 480 Da, ex: 480 nm/em: 530 nm), which was added to the culture prior to loading (as described for calcein). Co-cultures were subjected to 0.50 shear strain at a strain rate of 10 sec^{-1}, and neuronal versus

astrocytic rhodamine uptake was qualitatively assessed at 10 min post-insult ($n = 3$ cultures).

Assaying cell viability

Culture viability was assessed at 48 h following either shear or compressive loading (0.50 strain each) at strain rates of 1, 10, and 30 sec^{-1} or static control conditions ($n = 3$–7 cultures per group). Cell cultures were incubated with EthD-1 (4 μM) and calcein AM (2 μM; Molecular Probes) at 37°C for 30 min, and then rinsed with Dulbecco's phosphate-buffered saline. The percentage of surviving cells was calculated by counting the number of live cells (fluorescing green by AM-cleavage), and the number of cells with compromised membranes (dead or dying cells with nuclei fluorescing red by EthD-1). This assay is distinct from that described above because when AM is conjugated to calcein, it is lipid soluble and readily crosses the plasma membrane. AM cleavage occurs via esterase activity, which is indicative of metabolically active cells. Following this cleavage, the calcein fluoresces green (ex: 495 nm/em: 515 nm), and is trapped within the plasma membrane. The percentage of viable cells was based on the total number of cells present at the time point evaluated, and not on the total cells originally plated. Also, we have previously found that post-insult astrocyte proliferation can mask reductions in survival (Cullen et al., 2007b); therefore, we also calculated the density of dead cells normalized relative to the density of dead cells found in static control cultures.

Statistical analysis

Analysis of variance (ANOVA) was performed for the permeability and viability studies with deformation mode and level as independent variables. For culture level descriptions such as permeabilized cell density and cell viability, the n was the number of cultures per condition; whereas for cell-level comparisons of per-cell calcein uptake, the n was the number of cells measured from a given group (with cell sampling across multiple regions of interest and cultures for a given condition). When differences existed between groups, *post-hoc* Tukey's pair-wise comparisons were performed. Additionally, linear regression analyses were used to assess potential correlations between permeability measurements and subsequent culture viability. For all statistical tests, $p < 0.05$ was required for significance. Data are presented as mean ± standard deviation unless otherwise noted.

## Results

Shear versus compression permeability

3-D neuronal-astrocytic co-cultures were subjected to static (unloaded) conditions or bulk compressive or shear deformation (0.50 strain) at quasi-static (1 sec^{-1}) or dynamic (10 sec^{-1} or 30 sec^{-1}) strain rates. The normally cell-impermeant molecule calcein was utilized to evaluate non-physiological membrane disruptions following the prescribed loading conditions. Since calcein rinses out of cells if membrane integrity is not re-established, the presence of calcein$^+$ cells post-rinse directly indicates transient alterations in membrane permeability (i.e., membrane resealing). Minimal calcein uptake occurred under static control and quasi-static conditions (for both the shear and compression groups; Fig. 3A). However, there was increased calcein uptake following dynamic deformation, indicating that calcein diffused intracellularly and became sequestered during or within minutes following loading. The density of calcein$^+$ cells depended on strain rate ($p < 0.001$), but not the mode of deformation, and there were no significant interactions between these factors. Specifically, permeability increased as a function of strain rate, and was highest at 30 sec^{-1} for both compression and shear ($p < 0.05$). However, the density of calcein$^+$ cells did not vary between compression and shear at any of the matched strain rates (Fig. 3B). However, more calcein$^+$ cellular processes were observed following shear compared to compression. In order to present the density of calcein$^+$ cells in a broader context, the percentage of permeabilized cells was calculated normalized to the overall cell density in non-injured control cultures. This revealed that the percentage of calcein$^+$ cells in static and quasi-static control cultures was approximately < 1% and 3%, respectively. Following 10 sec^{-1} shear loading, approximately 10% of the cells were calcein$^+$ following shear deformation, compared to 1.5% following compression (not significant). Moreover, for 30 sec^{-1} conditions these levels rose to over 27% of cells following shear or compression.

To determine the degree of cell permeability, we evaluated the fluorescence intensity of calcein on a per-cell basis in the same cultures as above, revealing a significant increase in the mean intensity of calcein$^+$ cells strained at 30 sec^{-1} compared to quasi-static loading ($p < 0.05$) for both shear and compression (Fig. 3C). The mean intensity of calcein$^+$ cells was significantly increased at 10 sec^{-1} versus quasi-static shear loading ($p < 0.05$). Additionally, at a matched strain rate of 10 sec^{-1}, there was enhanced calcein uptake in cells following shear versus compression ($p < 0.05$; Fig. 3C).

Acute time course of permeability changes

Immediate alterations in cell membrane permeability were investigated on a cell-by-cell basis by imaging shear strain application in real-time. 3-D neuronal-astrocytic co-cultures were subjected to dynamic shear deformation (0.50 strain) in the presence of calcein. Immediately post-insult, a subset of cells became calcein$^+$ throughout the cell bodies, whereas in other cells a widespread loss of cell/process definition was apparent (Fig. 4A). These observations were quantified, revealing that roughly half (47.4%) of the cells showed no change (defined as < 10% change in intracellular fluorescence relative to background). Conversely, 42.1% of cells showed an immediate increase in intracellular intensity between 10 and 50%. Additionally, 10.5% of the cells had a > 50% change in intracellular intensity (these cells either blended with the background or appeared brighter than background). We then monitored calcein entry on a per-cell basis over time post-insult (Fig. 4B and C). Immediately following loading, intracellular (in somata as well as in processes) calcein intensity increased in a small portion of cells, consistent with earlier observations. However, in most cells a gradual increase in intracellular intensity was observed over minutes post-insult, leading to the somata and processes slowly blending into the background as calcein gradually diffused into the cells post-insult. These observations provide direct evidence of plasmalemma pores/tears as an immediate and direct result of high-strain-rate loading. Moreover, the relatively protracted diffusion over the acute period post-injury likely results in the
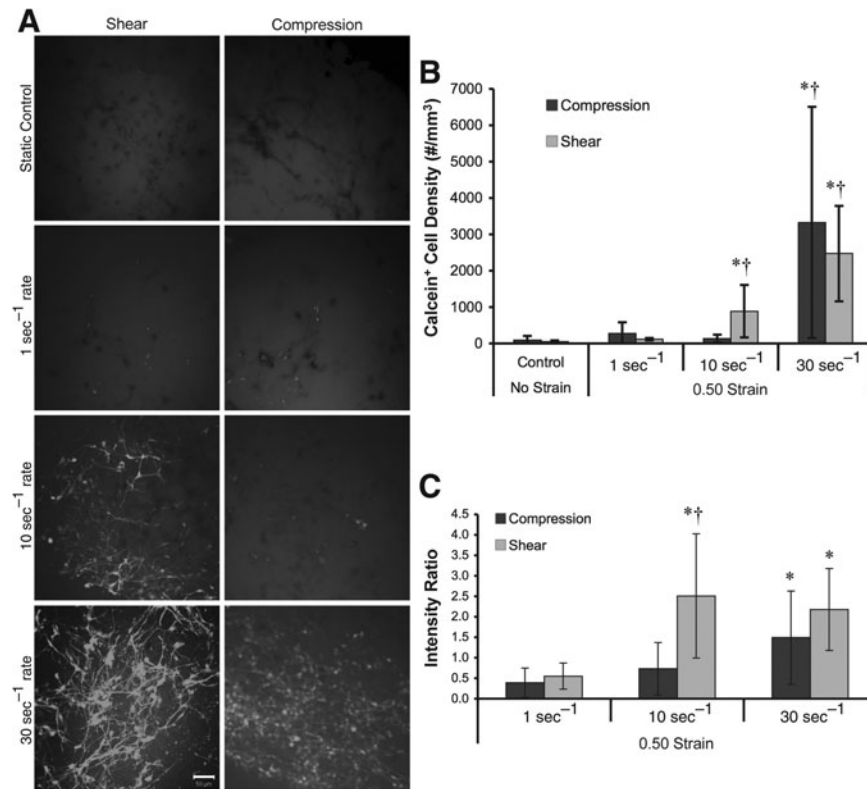
FIG. 3. Alterations in acute membrane permeability in shear versus compression. Representative confocal reconstructions of 3-D cultures following static control conditions or mechanical loading (0.50 strain at 1, 10, or 30 sec^{-1} strain rate; **A**). Calcein was added to the extracellular space prior to loading and enters permeable cells during or immediately following loading (reconstructions from 50-μm-thick z-stacks taken from cultures post-rinse; scale bar = 50 μm). Cell density of permeabilized (calcein$^+$) cells (**B**). The 3-D cell density and percentage of calcein$^+$ cells increased as a function of strain rate, and was highest at the maximum strain rate for both compressive and shear loading (*$p < 0.05$ versus static control; †$p < 0.05$ versus lower strain rates). The degree of cell permeability following variable rate shear or compressive (0.50 strain) loading (**C**). There was a significant increase in the mean intensity of calcein$^+$ cells versus quasi-static loading for both shear and compression at 30 sec^{-1} and shear only at 10 sec^{-1} (*$p < 0.05$). Also, at 10 sec^{-1} loading, there was enhanced calcein uptake following shear versus compression (†$p < 0.05$). Data are mean ± standard deviation.

substantial uptake observed following rinsing (as shown in Fig. 3).

The sub-acute time course of altered membrane permeability

The time-course of plasmalemma disruptions was investigated following shear loading at 0.50 strain, 10 sec^{-1} strain rate, by examining the density of permeabilized cells when permeability marker was added either pre-loading or at specific time points post-loading. Here, there was significant calcein uptake when present during loading; however, when calcein was added 10 min post-insult, there were few calcein$^+$ cells, indicating minimal uptake and/or retention (Fig. 5). To differentiate between acute resealing versus non-resealing, as well as delayed poration, we evaluated the density of cells post-insult using calcein and an additional membrane-impermeant marker, EthD-1. Calcein and EthD-1 are complementary permeability markers as used here, since calcein requires resealing for intracellular sequestration post-rinse, whereas EthD-1 irreversibly binds DNA and will thus label compromised cells regardless of membrane resealing. Here,

calcein was added pre-insult (to track calcein sequestration over time), but EthD-1 was added either pre-insult or at 10 min or 60 min post-insult (to assess potential membrane resealing and secondary poration, imaging occurred 10 min after EthD-1 addition following rinse). This revealed that both the density of calcein$^+$ and EthD-1$^+$ cells varied over time post-insult. In particular, the density of EthD-1$^+$ cells increased immediately after the insult, decreased precipitously when added 10 min post-insult, but then began increasing again at 60 min (Fig. 6). This increasing trend in EthD-1$^+$ cells led to a twofold increase by 6 h post-insult (data not shown). In addition, the density of calcein$^+$ cells increased at 20 min post-insult, possibly due to intracellular diffusion of calcein and/or persistent uptake in processes remote from the somata. Also, by 60 min post-insult, calcein$^+$ cellular debris was present, potentially indicating active removal of calcein or the breakdown of some initially calcein$^+$ cells. Moreover, at the earliest time point a subset of cells was co-labeled with calcein and EthD-1. Collectively, these observations demonstrate that there is a primary, transient phase of physical poration (i.e., "mechanoporation"), that concludes within minutes, or perhaps tens of seconds, of loading. Also, these results suggest a phase of secondary
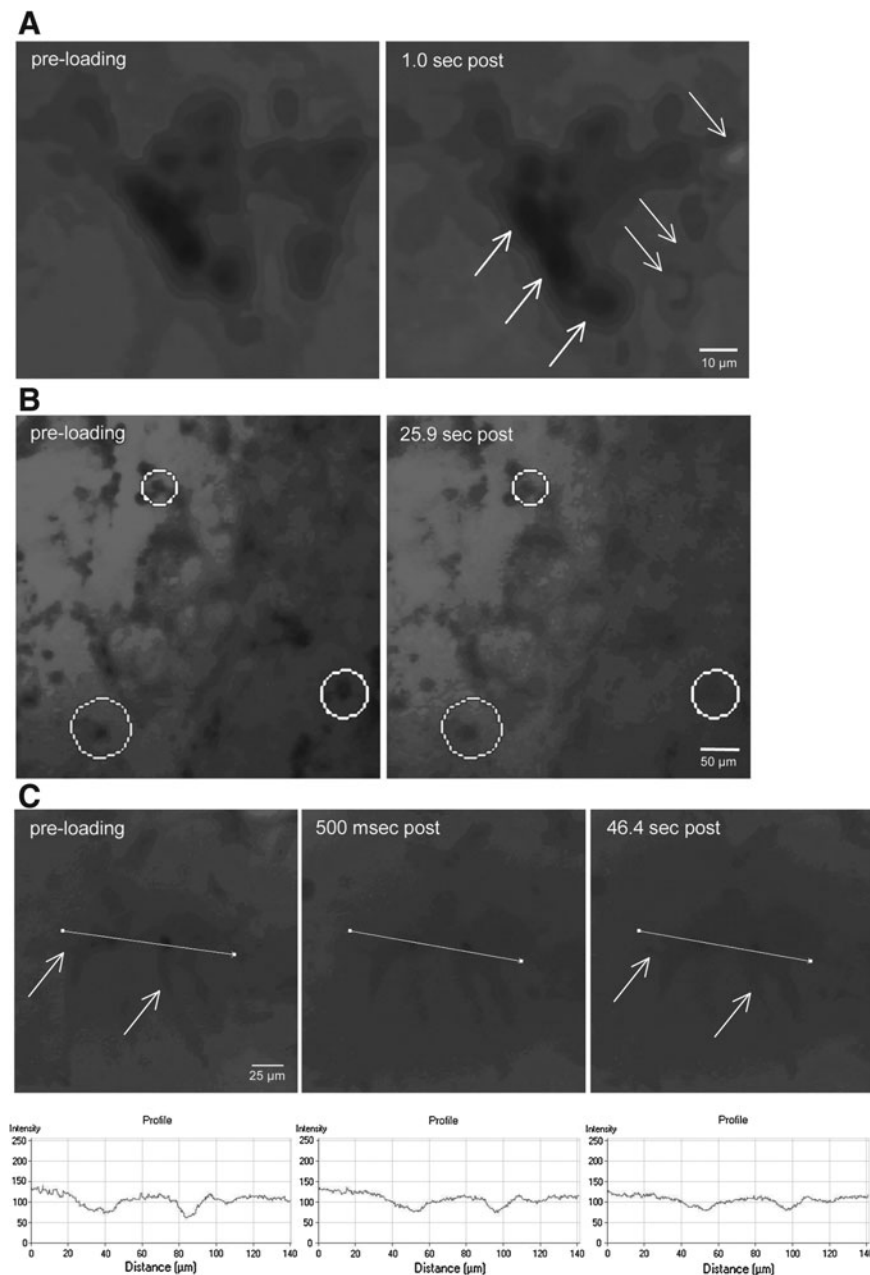
FIG. 4. Real-time analyses of calcein uptake following shear deformation. The shear deformation device permits real-time imaging across the 3-D cultures before, during, and after loading. Calcein diffused throughout the extracellular space prior to loading (resulting in relatively high fluorescence background during imaging). The 3-D cultures were dynamically deformed at 0.50 shear strain ($10\,sec^{-1}$ or $30\,sec^{-1}$ strain rate). Pre-loading, there were clear margins delineating neural somata and processes, indicating intact plasmalemma. However, immediately post-insult, there was a subset of cells that became calcein$^+$ (white arrows in **A**), whereas some cells excluded calcein (black arrows in **A**). In other cases, a widespread loss of definition was apparent in neurites as well as somata (**B**). Calcein uptake was tracked on a per-cell basis throughout loading (**C**). Within 500 msec post-insult, intracellular calcein intensity increased. This process continued throughout the first minute, resulting in processes gradually blending with the background (white arrows in **C**).

poration possibly represented by persistent, cycling, or permanent pores and/or the initiation of cell death.

Neuronal versus astrocytic permeability changes

Acute trauma-induced alterations in membrane permeability were investigated in neurons versus astrocytes following shear loading at 0.50 strain at $10\,sec^{-1}$. For these studies, a group of 3-D co-cultures were generated using GFP$^+$ neurons mixed with wild-type astrocytes to permit neuronal identification, and a red permeability marker, rhodamine, was used. Qualitative assessment revealed that alterations in membrane permeability occurred in both neurons (GFP$^+$/rhod$^+$) and astrocytes (GFP$^-$/rhod$^+$), with robust rhodamine uptake in both the somata and cellular processes (Fig. 7).
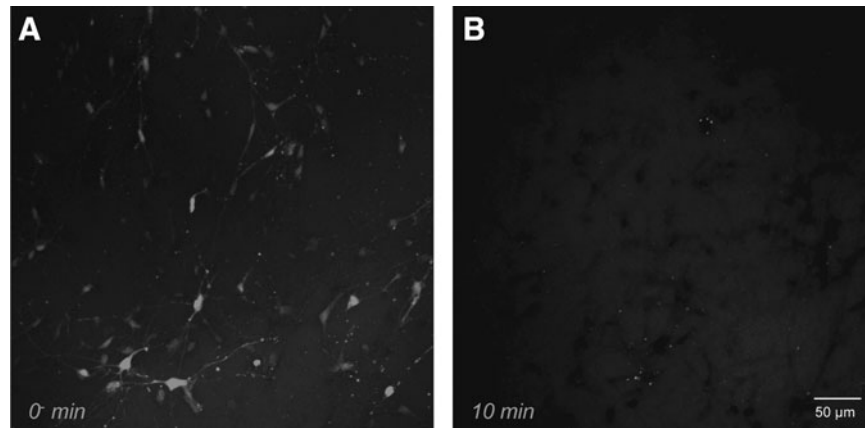
FIG. 5. Sub-acute permeability alterations. Representative confocal reconstructions of 3-D neuronal-astrocytic co-cultures following mechanical loading at 0.50 shear strain, $10 \sec^{-1}$ strain rate. Calcein was added to the cultures either prior to loading (0^-, **A**), or 10 min post-loading (**B**). There was modest uptake when the calcein was present during loading, but minimal uptake when calcein was added minutes post-insult (reconstructions from 50-μm-thick z-stacks imaged post-rinse).

Shear versus compression viability

At 48 h post-insult, we evaluated the consequences of traumatic loading on cell survival (Fig. 8A). Following static control conditions or mechanical loading (0.50 shear or compressive strain at 1, 10, or $30 \sec^{-1}$ strain rate), the percentage of viable cells depended significantly on strain rate ($p < 0.01$) but not the mode of deformation, with no significant interaction between these factors. In particular, following shear loading, the percentage of viable cells was significantly reduced at $30 \sec^{-1}$ versus quasi-static ($1 \sec^{-1}$) or static loading ($p < 0.05$; Fig. 8B). We have previously shown that a mechanical insult may directly initiate astrocyte proliferation (Cullen et al., 2007b), making the density of dead cells a more accurate marker of post-injury survival. The fold-increase in the density of dead cells (compared to static controls) varied significantly based on strain rate ($p < 0.05$) as well as deformation mode ($p < 0.001$), with no significant interaction between these factors. Specifically, following shear loading at $10 \sec^{-1}$ or $30 \sec^{-1}$, the density of dead cells increased by over fivefold ($p < 0.05$; Fig. 8C). Additionally, at matched strain rates of $10 \sec^{-1}$ and $30 \sec^{-1}$, there were significant increases in cell death in shear versus compression ($p < 0.05$ each; Fig. 8C).

Correlation between permeability and viability

Linear regression analyses were performed to assess the potential relationship between acute cell damage and subsequent cell death. Specifically, the density of compromised cells (calcein$^+$), and the degree of per-cell calcein uptake measured at 10 min post-insult were correlated with the density of dead cells across loading conditions at 48 h post-insult. The density of permeabilized cells correlated poorly, with later cell death following shear loading ($R^2 = 0.22$). In contrast, this parameter correlated strongly with cell death following compressive loading ($R^2 = 0.98$; Fig. 9A); however, there was a lack of distinction between quasi-static and $10 \sec^{-1}$ loading. Alternatively, the degree of per-cell calcein uptake, potentially proportional to the degree of cell damage, correlated strongly with cell death for both shear and compression ($R^2 = 0.96$ and $R^2 = 0.95$, respectively; Fig. 9B). Ad-

ditionally, the increase in cell death was markedly greater with respect to strain rate for shear versus compression, suggesting that shear deformation is the prevalent mechanism of cellular damage that ultimately induces cell death. Taken together, these results indicate that the degree of initial transient structural compromise was a stronger predictor of cell death than the number of compromised cells.

Discussion

Traumatic loading to the brain results in complex strain fields; therefore, we imparted controlled shear and compressive deformation to a 3-D neural culture model, which was chosen due to similarities to *in vivo* cytoarchitecture. Using defined inputs to a heterogeneous, anisotropic 3-D network of cells is intended to represent a spatial range of deformation patterns (i.e., shear- or compression-dominated) that may occur at different locations or in varying loading directions within the brain during a traumatic insult. We subjected 3-D neural co-cultures to mechanical loading (0.50 shear or compressive strain at 1, 10, or $30 \sec^{-1}$ strain rate) or static control conditions in order to investigate acute and sub-acute plasma membrane disruptions and cell viability. Our major findings were as follows: (1) disruptions of the plasmalemma occurred immediately upon shear or compressive loading and persisted over seconds; (2) the loading thresholds for these acute plasmalemma disruptions were lower following shear versus compression ($\geq 10 \sec^{-1}$ in shear; $\geq 30 \sec^{-1}$ in compression), with shear resulting in an increased degree of per-cell failure and increased compromise of cellular processes; (3) acute alterations in membrane permeability occurred in both neurons and astrocytes; (4) membrane compromise was bi-phasic over minutes to hours post-insult, with acute disruptions immediately upon loading which resealed rapidly in most cases, followed by secondary loss of membrane integrity; and (5) both shear and compressive loading induced cell death by 48 h post-insult, with shear resulting in significantly higher cell death than compression, when loaded at a relatively high strain rate.

Acute plasma membrane compromise following mechanical loading was found to be strain rate-dependent, consistent
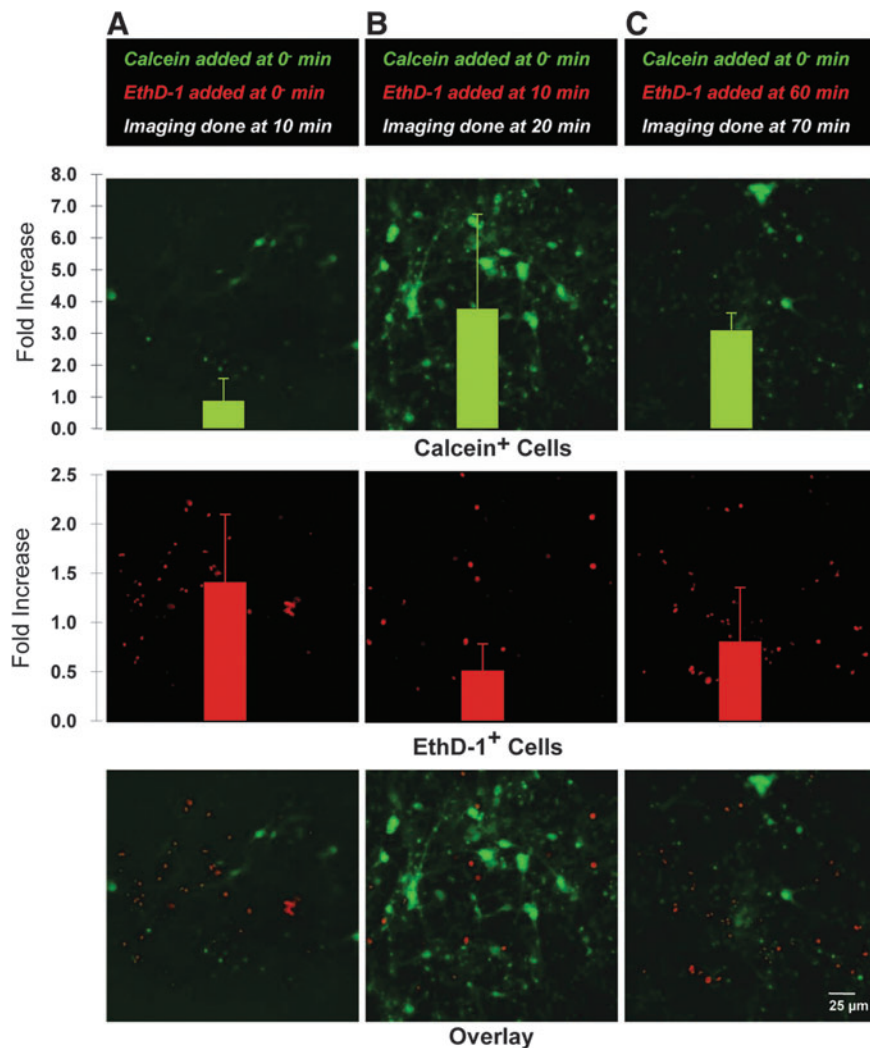
FIG. 6. Sub-acute time course of permeability alterations. Representative confocal reconstructions of 3-D neuronal-astrocytic co-cultures following mechanical loading at 0.50 shear strain, $10 \sec^{-1}$ strain rate. Calcein was added to the cultures only prior to loading (0^-), whereas EthD-1 was added either prior to loading (**A**, imaging done at 10 min), or 10 min (**B**, imaging done at 20 min), or 60 min (**C**, imaging done at 70 min) post-loading (reconstructions from 60-μm-thick z-stacks imaged post-rinse). Permeabilized cells were quantified and normalized to the density of calcein$^+$ or EthD-1$^+$ cells in static control cultures. Over 10 min, intracellular calcein increased (**B**); however, this was followed by a decrease in intracellular calcein by 60 min with indications of cellular debris (**C**), suggesting a second phase of altered permeability. In contrast, when EthD-1 was added 10 min post-insult, there was a decrease in EthD-1$^+$ cells (**B**), compared to the earlier time point (**A**), but began to increase again gradually over hours post-insult (**C**), suggesting a bi-phasic response. Data are mean ± standard deviation (EthD-1, ethidium homodimer-1).

with previous studies (Cullen et al., 2007b; Geddes et al., 2003; LaPlaca et al., 1997; Prado et al., 2005). This behavior can be partially explained by the viscoelastic nature of cells, which predicts that for high strain rate loading, characteristic of traumatic neural injury, the elastic component will dominate, causing cells to behave in a more rigid manner (i.e., failure given sufficiently large deformation). On the other hand, low strain rate loading primarily engages the viscous component, whereby structural components are able to comply with even large deformations (Galbraith et al., 1993). Remarkably, we observed virtually no changes in membrane permeability when even large-deformation −0.50 compression or shear strain occurred slowly (applied over 500 msec). Moreover, we found that the degree of calcein uptake per permeabilized cell,

potentially a gauge of local stress/strain concentrations, increased in a strain rate-dependent manner. A noteworthy caveat in this analysis is that calcein will not necessarily stain all permeabilized cells, since it will not be retained in cells that were permeabilized but not resealed. Likewise, pores smaller than a critical diameter will prevent calcein entry, which may also be affected by molecular charge, shape, and binding affinity. Thus, additional studies of the nature of mechanically-induced membrane damage may require alternative permeability markers with a range of defined characteristics.

The acute cellular responses in 3-D cultures exposed to bulk shear or compression has relevance to loading profiles in TBI (see Fig. 1). We did not find significant differences in the density of permeabilized cells between these two bulk modes
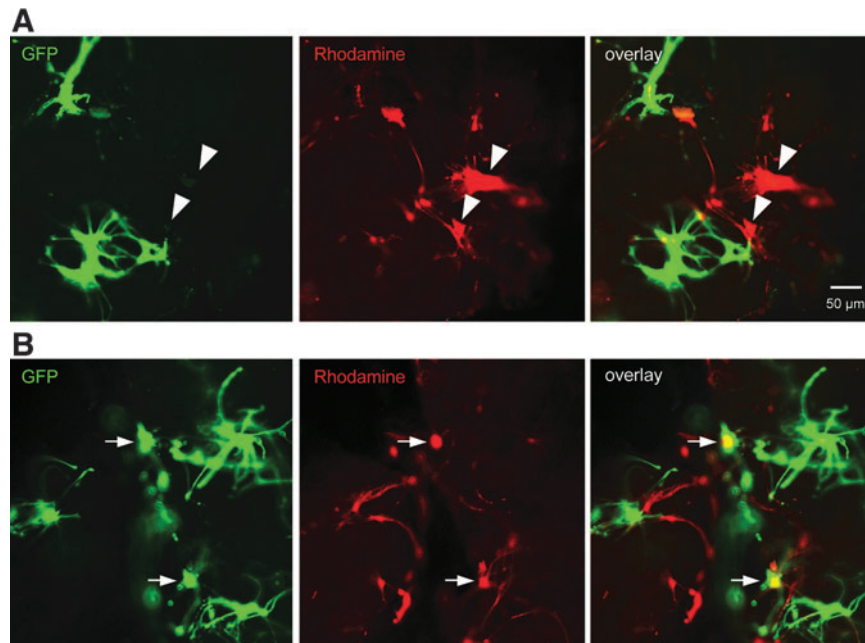
FIG. 7. Trauma-induced alterations in membrane permeability in neurons versus astrocytes. A subset of co-cultures was generated using green fluorescent protein[+] (GFP^{+}) neurons mixed with wild-type astrocytes to permit neuronal identification, and a red permeability marker was utilized (rhodamine). Here, there was a mix of both rhod[+]/GFP[−] astrocytes (denoted by arrowheads in **A**), and rhod[+]/GFP^{+} neurons (denoted by arrows in **B**), exhibiting altered membrane permeability following injury. This demonstrated the susceptibility of both cell types to acute plasmalemma disruptions following dynamic loading.

of deformation at matched strain rates. However, the degree of damage (i.e., calcein uptake) on a per-cell basis was greater following shear deformation than compression deformation. Shear conditions led to increased calcein uptake at lower strain rates, demonstrating a lower threshold for membrane permeability following shear versus compression. Moreover, we observed more calcein in cellular processes following shear versus compression, indicating that cellular processes are either more vulnerable to shear loading, or increased somatic permeability leads to enhanced diffusion to the processes. The ramifications of immediate plasmalemma compromise may be devastating, triggering the loss of electrochemical potential, transport, osmotic imbalance, and cell rupture (Bartoletti et al., 1989). The resulting loss of ionic homeostasis, particularly Ca^{2+} homeostasis, has been shown to disrupt action potential firing and synapse function, impair axonal conduction, and play a role in excitotoxicity, cytoskeletal breakdown, mitochondrial dysfunction, necrosis, and apoptosis (Dumont et al., 2001; Galbraith et al., 1993; Goforth et al., 1999; LaPlaca et al., 1997; McIntosh et al., 1998; Raghupathi, 2004; Rami et al., 1997; Shi and Whitebone, 2006; Villa et al., 1998; Weber et al., 1999,2004; Zhang et al., 1996).

We also investigated the mechanisms of strain-induced membrane disruption by imaging permeability dynamics in real time, revealing at least three subpopulations of cells with regard to calcein uptake, despite a uniform bulk insult. One subpopulation showed calcein uptake from the extracellular space immediately upon deformation, another subpopulation showed gradual calcein uptake over tens of seconds to minutes, and a third subpopulation showed no calcein uptake even over minutes post-insult. Local cellular strains are

functions of cell morphology and orientation (Cullen and LaPlaca, 2006), and therefore it is not surprising to observe this heterogeneous response within 3-D cultures. These responses vary due to possible differences in the following: cell morphologies (affecting stress concentrations and potentially relating to cell mechanical properties), orientation of somata/processes with respect to the bulk strain field (affecting principal axes of local cellular strains), and/or number of cellular processes (affecting the complexity of the strain field). In addition, these results may indicate local differences in mechanical properties and thus cell tolerances (Elkin and Morrison, 2007; Elkin et al., 2007), and is consistent with other studies that suggest that multiple types of primary neuronal and axonal injury co-exist following trauma (Farkas and Povlishock, 2007; Farkas et al., 2006; Kelley et al., 2006; Singleton and Povlishock, 2004; Stone et al., 2004).

Additionally, we investigated the sub-acute time course of alterations in membrane permeability discriminating between cells that were transiently porated (labeled using a marker requiring resealing for intracellular sequestration: calcein), and cells with transient or prolonged poration (labeled using a marker that binds an intracellular substrate: EthD-1). Although we found significant numbers of permeable cells at the time of injury, membrane integrity was re-established by 10 min post-injury, as previously reported (Geddes et al., 2003; Prado et al., 2005). Additionally, cells that became calcein[+] at the time of injury became "leaky" within 1 h, suggesting that some initially compromised cells developed a second phase of membrane compromise due to secondary processes, potentially a progression towards cell death. Likewise, based on the number of EthD-1^{+} cells, intracellular access of EthD-1 spiked immediately post-insult
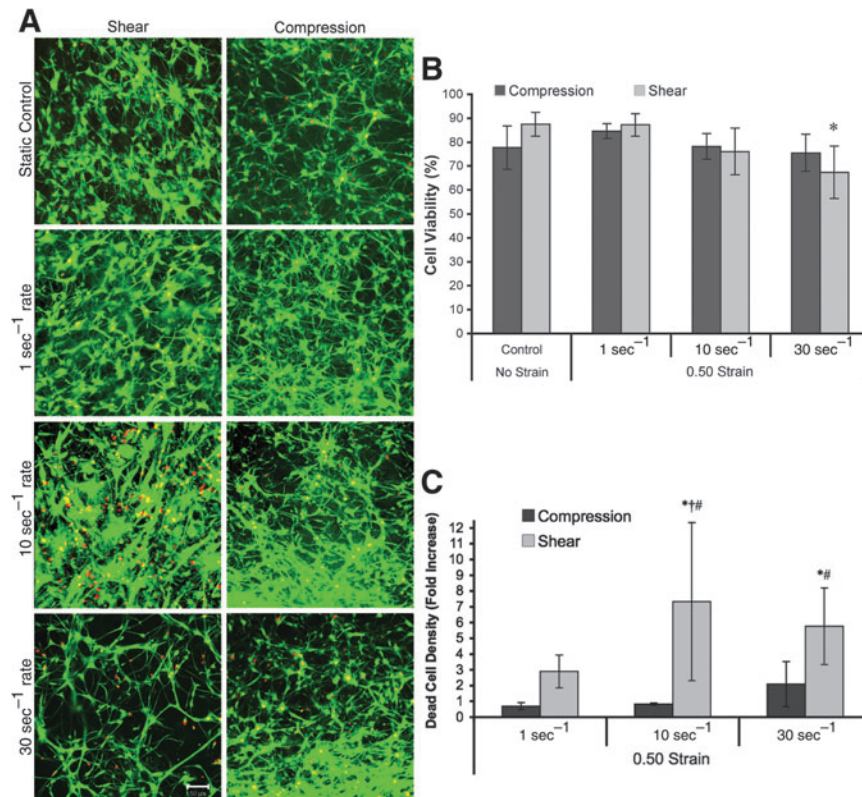
FIG. 8. Post-insult viability in shear versus compression. Representative confocal reconstructions of culture viability following static control conditions or mechanical loading (0.50 strain at 1, 10, or $30\,sec^{-1}$ strain rate; **A**). Live cells are green and the nuclei of dead/dying cells are red (reconstructions from 100-μm-thick z-stacks; scale bar$=50\,\mu$m). Percentage of viable cells (**B**). The percentage of viable cells 48 h following shear deformation depended significantly on injury level (*$p<0.05$ versus static and quasi-static controls). Dead-cell density (**C**). Post-insult proliferation may mask reductions in survival, thus the density of dead cells was calculated (normalized relative to static controls). The density of dead cells varied significantly based on injury level ($p<0.05$), as well as deformation mode ($p<0.001$). Pair-wise comparisons: *$p<0.05$ versus static control; †$p<0.05$ versus quasi-static; #$p<0.05$ versus matched strain rate). Data are mean$\pm$standard deviation.

when EthD-1 was present during injury, but decreased when EthD-1 was added 10 min post-injury. This trend then reversed as EthD-1$^+$ cells began increasing by 60 min and continued to increase out to at least 6 h. This increased cellular uptake of EthD-1 over hours post-injury also suggests a secondary, developing phase of membrane compromise which may include dying or dead cells. This cell population may consist of initially compromised cells that experienced secondary membrane damage, or cells that were affected by the mechanical insult independent from acute mechanoporation. The precise mechanisms of secondary membrane permeability are of great interest to the subject of persistent cell damage, but are beyond the scope of the current study.

Of note, EthD-1 is commonly used to identify dead cells, because live cells have intact membranes and thus are able to exclude it. Implicit in this distinction is that a compromised plasmalemma indicates a dead or dying cell. Our results suggest that EthD-1 may be used as a marker of membrane permeability at acute time points, because despite no cell loss in the first hour post-insult, EthD-1 labeled cells immediately and at 60 min after loading, while cells exclude EthD-1 (and calcein) when added 10 min after the insult. Similarly to our use of EthD-1 as a membrane permeability marker, other studies have used propidium iodide (Whalen et al., 2008), and ethidium bromide (Koob et al., 2005), both irreversible DNA

binding dyes commonly used for identifying dead cells, as markers of membrane permeability following TBI.

In light of the many potentially damaging consequences of high strain rate deformation, we evaluated cell survival within the 3-D co-cultures 48 h after traumatic loading. There were significant reductions in cell viability after high ($30\,sec^{-1}$) strain rate loading compared to quasi-static ($1\,sec^{-1}$) loading or static control cultures, indicating a strain rate-dependence for post-insult survival. We found an over fivefold increase in cell death following $10\,sec^{-1}$ and $30\,sec^{-1}$ shear strain loading, but only a twofold increase in cell death following $30\,sec^{-1}$ compressive loading. We further correlated two acute responses with subsequent cell death: (1) the density of permeabilized cells, and (2) the degree of per-cell permeability changes. For both strain modes, the degree of acute permeability was a stronger predictor of cell death than the density of permeabilized cells. These results implicate the degree of damage rather than the presence of damage in trauma-induced cell death. Possibly, increased severity of initial structural compromise may directly predispose a cell to death, whereas less severe compromise is survivable. Alternatively, different populations of cells may subsequently die, which is unknown, given we did not track individual cells over the 48-h period. Indeed, calpain-mediated spectrin proteolysis, an indicator of necrotic cell death, has been shown to
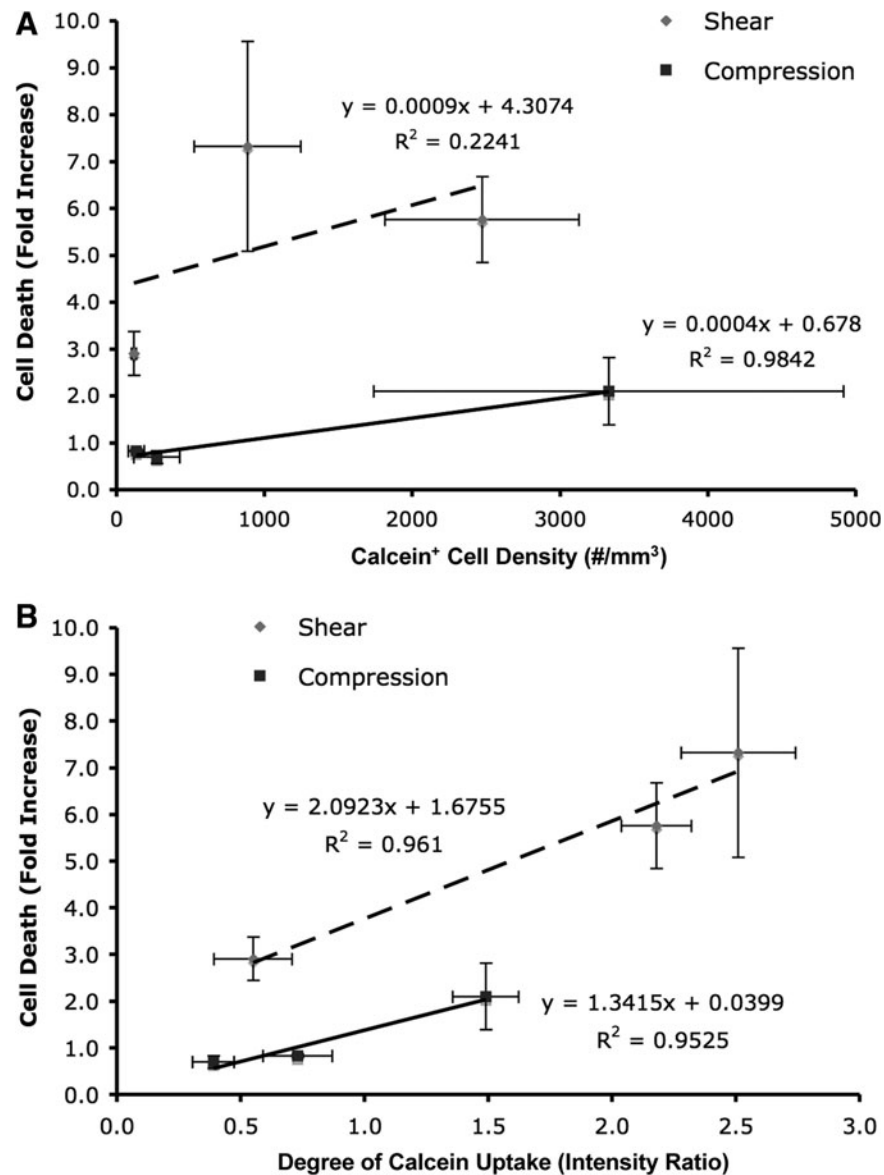
FIG. 9. Regression analyses to assess potential correlations between acute markers of cell damage and subsequent longer-term cell death. Cell death versus the density of permeabilized cells **(A)** or versus the degree of per-cell permeability **(B).** The degree of calcein uptake on a per cell basis (B) was a stronger indicator of cell death than the density (or percentage) of calcein^{+} cells (A), implicating the degree of damage rather than the presence of damage in subsequent cell death. Additionally, this increase in cell death was markedly greater for shear versus compression across all strain rates, substantiating that shear deformation is the prevalent mechanism of cellular damage that ultimately induces cell death. Data: mean±SEM.

occur independent of membrane disruption *in vivo* (Farkas et al., 2006). Also, neural cell survival following early post-traumatic permeability increases has also been observed (Farkas et al., 2006; Singleton and Povlishock, 2004). Thus, these studies suggest that many initially permeabilized cells survive the insult; however, there may be prolonged alteration in physiology or later death in this population. Not surprisingly, there is also evidence of delayed cell death in cells that initially survive membrane compromise *in vivo* (Whalen et al., 2008). Thus, the long-term survivability of initially permeabilized cells, as well as the functional state of these cells, is not completely understood and warrants further investigation.

Notably, the finding that neural cellular outcomes are more detrimental following shear than compression was substantiated based on multiple lines of experimentation, including post-injury cell permeability (Fig. 3) and cell death (Fig. 8), as well as in relationships between these parameters (Fig. 9). However, this result is not surprising given that the bulk mode of deformation may in fact produce heterogeneous cellular loading conditions. We chose to compare a 0.50 bulk strain magnitude based on controllable loading conditions in shear or compression. We have previously shown that a strain magnitude of 0.50 produces significant cell death in shear loading, and therefore considered this level sufficiently injurious for comparisons to compression. Although we were able
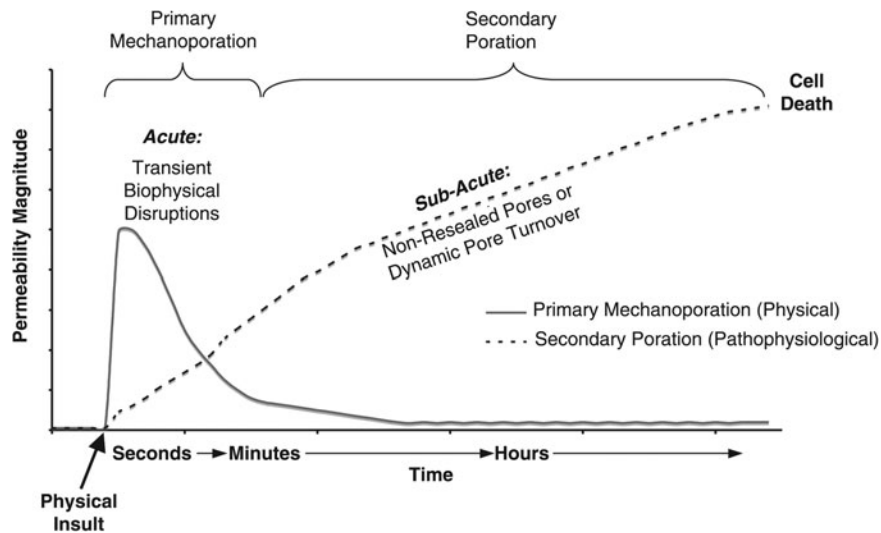
FIG. 10. Postulated cell membrane permeability mechanisms and time course. Converging evidence suggests that the primary phase of physical membrane poration (nano- to micro-tears, defined as "mechanoporation") ends within seconds of the biomechanical loading, and thus is often marked by transient, acute biophysical disruptions. A protracted phase of secondary poration ensues over time in some cell populations. This second phase of membrane permeability/poration is likely enzymatically-mediated and potentially marked by dynamic pore turnover that may ultimately lead to cell death. Collectively, these two related yet distinct mechanisms yield the appearance of bi-phasic alterations in membrane permeability over the first several hours post-insult.

to match overall strain with our custom device, we acknowledge that the actual strain fields applied at the cellular level may be different. This underlines an important point: neural cellular tolerances, while often determined using a prescribed strain magnitude and strain rate, are complex and will likely vary based on the dominant strain modality, as well as the complexity of the loading among heterogeneous cell components (Cullen and LaPlaca, 2006; Geddes-Klein et al., 2006). Moving forward, this work may be expanded to further delineate tissue-level shear and compressive tolerance curves based on a wider range of loading magnitudes and rates. In addition, because the local cellular strain fields are complex 3-D strain tensors based on cell orientation with respect to the bulk loading and number of neurites with distinct departure trajectories, relating the acute permeability fate of a particular cell based on the specific cell strain characteristics would yield valuable 3-D cell-level threshold data. This will require computational analyses and cellular position/excursion measurements based on the range of morphologies and orientations that are beyond the scope of the current study.

Overall, our data suggest that many of the initial disruptions in the plasma membrane are repaired within minutes (perhaps seconds) of injury. Repair mechanisms may include lowering the thermodynamic state of the lipid bilayer to reseal ruptures, and/or calcium-dependent vesicle-membrane fusion (Chang and Reese, 1990; Miyake and McNeil, 1995; McNeil et al., 2000,2003; Nehrt et al., 2007; Schlicher et al., 2006; Shi et al., 2001). Some of these emergency cellular repair mechanisms may be energetically taxing (Togo et al., 2000), and may occur when metabolic demands in the injured cell are increasing. These reparative mechanisms may then be limited or not available as secondary degradative events are initiated, such as calcium-dependent activation of proteases and phospholipases that may enzymatically digest the cytoskeleton and plasma membrane (Büki et al., 1999; Homayoun et al., 2000;

Lyeth et al., 1996; Saatman et al., 2003; Serbest et al., 2007), thus causing a secondary poration. Although these secondary mechanisms of cell damage are not unique to trauma (Adibhatla and Hatcher, 2008; Vosler et al., 2008), primary (physical) damage as well as the damaged/reparative context in which the secondary events ensue are unique to trauma.

Collectively, our observations lead us to postulate a biphasic time course of events involving post-trauma alterations in membrane permeability that may ultimately lead to cell death (Fig. 10). As a direct physical consequence of traumatic loading, a primary phase of mechanoporation lasting seconds to minutes post-injury is initiated in a subset of cells. In some cases, this may be irreparable damage, while in other cases this phase is marked by transient disruption. In cells that are able to reseal, the initial physical insult may provide sufficient perturbation to lead to a secondary (sub-acute) phase of membrane damage ensuing in the hours post-injury, likely due to non-mechanical causes (e.g., phospholipase and calpain activation). Thus, over at least the first hour post-insult, two related yet distinct mechanisms of membrane damage appear as biphasic alterations in membrane permeability.

In summary, our findings demonstrate mechanisms of acute damage to neural cells following high rate mechanical loading. There was a particular vulnerability to shear deformation, which resulted in increased cell structural damage/failure and death compared to compression. We observed a biphasic response in cell membrane permeabilization upon injury, with a primary mechanoporation phase lasting seconds to minutes post-injury, and a secondary phase of membrane damage ensuing in the hours post-injury. These results are the basis for a proposed sequence of membrane damage and repair dynamics that should be considered in light of other consequences of mechanical injury for both neural and other systems, as mechanoporation may be a key trigger for cellular dysfunction. In addition, elucidation of acute mechanisms of

structural damage using biomechanically-characterized reduced (i.e., *in vitro*) models can then be extrapolated to cellular or tissue loading responses in human TBI, and/or used in conjunction with computer simulations and animal studies. Further investigation of these events and their time course will contribute to our increased understanding of cellular tolerances, and be useful in predicting damage in response to large-magnitude, high-rate deformation.

Acknowledgments

Author Disclosure Statement

No competing financial interests exist.

References

Adibhatla, R., and Hatcher, J. (2008). Phospholipase A2, reactive oxygen species, and lipid peroxidation in CNS pathologies. BMB Rep. 41, 560–567.

Adibhatla, R.M., Hatcher, J.F., and Dempsey, R.J. (2006). Lipids and lipidomics in brain injury and diseases. AAPS J. 8, E314–E321.

Bartoletti, D.C., Harrison, G.I., and Weaver, J.C. (1989). The number of molecules taken up by electroporated cells: quantitative determination. FEBS Lett. 256, 4–10.

Büki, A., Siman, R., Trojanowski, J., and Povlishock, J. (1999). The role of calpain-mediated spectrin proteolysis in traumatically induced axonal injury. J. Neuropathol. Exper. Neurol. 58, 365–375.

Chang, D.C., and Reese, T.S. (1990). Changes in membrane structure induced by electroporation as revealed by rapid-freezing electron microscopy. Biophys. J. 58, 1–12.

Cullen, D.K., and LaPlaca, M.C. (2006). Neuronal response to high rate shear deformation depends on heterogeneity of the local strain field. J. Neurotrauma 23, 1304–1319.

Cullen, D.K., Lessing, M.C., and LaPlaca, M.C. (2007a). Collagen-dependent neurite outgrowth and response to dynamic deformation in three-dimensional neuronal cultures. Ann. Biomed. Eng. 35, 835–846.

Cullen, D.K., Simon, C.M., and LaPlaca, M.C. (2007b). Strain rate-dependent induction of reactive astrogliosis and cell death in three-dimensional neuronal-astrocytic co-cultures. Brain Res. 1158, 103–115.

Cullen, D.K., Wolf, J.A., Vernekar, V.N., Vukasinovic, J., and LaPlaca, M.C. (2011). Neural tissue engineering and biohy-

bridized microsystems for neurobiological investigation in vitro (part 1). Crit. Rev. Biomed. Engineering 39, 201–240.

Dumont, R.J., Verma, S., Okonkwo, D.O., Hurlbert, R.J., Boulos, P.T., Ellegala, D.B., and Dumont, A.S. (2001). Acute spinal cord injury, part II: contemporary pharmacotherapy. Clin. Neuropharmacol. 24, 265–279.

Elkin, B.S., Azeloglu, E.U., Costa, K.D., and Morrison, B., 3rd (2007). Mechanical heterogeneity of the rat hippocampus measured by atomic force microscope indentation. J. Neurotrauma 24, 812–822.

Elkin, B.S., and Morrison, B., 3rd (2007). Region-specific tolerance criteria for the living brain. Stapp Car Crash J. 51, 127–138.

Farkas, O., Lifshitz, J., and Povlishock, J.T. (2006). Mechanoporation induced by diffuse traumatic brain injury: an irreversible or reversible response to injury? J. Neurosci. 26, 3130–3140.

Farkas, O., and Povlishock, J.T. (2007). Cellular and subcellular change evoked by diffuse traumatic brain injury: a complex web of change extending far beyond focal damage. Prog. Brain Res. 161, 43–59.

Galbraith, J.A., Thibault, L.E., and Matteson, D.R. (1993). Mechanical and electrical responses of the squid giant axon to simple elongation. J. Biomech. Eng. 115, 13–22.

Geddes, D.M., Cargill, R.S., 2nd, and LaPlaca, M.C. (2003). Mechanical stretch to neurons results in a strain rate and magnitude-dependent increase in plasma membrane permeability. J. Neurotrauma 20, 1039–1049.

Geddes-Klein, D.M., Schiffman, K.B., and Meaney, D.F. (2006). Mechanisms and consequences of neuronal stretch injury in vitro differ with the model of trauma. J. Neurotrauma 23, 193–204.

Gennarelli, T.A. (1993). Mechanisms of brain injury. J. Emerg. Med. 11 Suppl. 1, 5–11.

Goforth, P.B., Ellis, E.F., and Satin, L.S. (1999). Enhancement of AMPA-mediated current after traumatic injury in cortical neurons. J. Neurosci. 19, 7367–7374.

Hatten, M.E., Liem, R.K., Shelanski, M.L., and Mason, C.A. (1991). Astroglia in CNS injury. Glia 4, 233–243.

Holbourne, A. (1943). Mechanics of head injury. Lancet 2, 438–441.

Homayoun, P., Parkins, N., Soblosky, J., Carey, M., Rodriguez de Turco, E., and Bazan, N. (2000). Cortical impact injury in rats promotes a rapid and sustained increase in polyunsaturated free fatty acids and diacylglycerols. Neurochem. Res. 25, 269–276.

Irons, H.R., Cullen, D.K., Shapiro, N.P., Lambert, N.A., Lee, R.H., and LaPlaca, M.C. (2008). Three-dimensional neural constructs: a novel platform for neurophysiological investigation. J. Neural Eng. 5, 333–341.

Kelley, B.J., Farkas, O., Lifshitz, J., and Povlishock, J.T. (2006). Traumatic axonal injury in the perisomatic domain triggers ultrarapid secondary axotomy and Wallerian degeneration. Exp. Neurol. 198, 350–360.

Kleinman, H., McGarvey, M., Hassell, J., Star, V., Cannon, F., Laurie, G., and Martin, G. (1986). Basement membrane complexes with biological activity. Biochemistry 25, 312–318.

Koob, A.O., Duerstock, B.S., Babbs, C.F., Sun, Y., and Borgens, R.B. (2005). Intravenous polyethylene glycol inhibits the loss of cerebral cells after brain injury. J. Neurotrauma 22, 1092–1111.

LaPlaca, M.C., Cullen, D.K., McLoughlin, J.J., and Cargill, R.S., 2nd (2005). High rate shear strain of three-dimensional neural cell cultures: a new in vitro traumatic brain injury model. J. Biomech. 38, 1093–1105.

LaPlaca, M.C., Lee, V.M., and Thibault, L.E. (1997). An in vitro model of traumatic neuronal injury: loading rate-dependent changes in acute cytosolic calcium and lactate dehydrogenase release. J. Neurotrauma 14, 355–368.

LaPlaca, M.C., Simon, C.M., Prado, G.R., and Cullen, D.K. (2007). CNS injury biomechanics and experimental models. Prog. Brain Res. 161, 13–26.

Liao, S.L., and Chen, C.J. (2001). Tyrosine kinase signaling involved in glutamate-induced astrocyte proliferation. Neuroreport 12, 3519–3522.

Lyeth, B., Gong, Q., Dhillon, H., and Prasad, M. (1996). Effects of muscarinic receptor antagonism on the phosphatidylinositol bisphosphate signal transduction pathway after experimental brain injury. Brain Res. 742, 63–70.

Margulies, S., and Hicks, R. (2009). Combination therapies for traumatic brain injury: prospective considerations. J. Neurotrauma 26, 925–939.

Margulies, S.S., and Thibault, L.E. (1992). A proposed tolerance criterion for diffuse axonal injury in man. J. Biomech. 25, 917–923.

McIntosh, T.K., Saatman, K.E., Raghupathi, R., Graham, D.I., Smith, D.H., Lee, V.M., and Trojanowski, J.Q. (1998). The Dorothy Russell Memorial Lecture. The molecular and cellular sequelae of experimental traumatic brain injury: pathogenetic mechanisms. Neuropathol. Appl. Neurobiol. 24, 251–267.

McNeil, P.L., Miyake, K., and Vogel, S.S. (2003). The endomembrane requirement for cell surface repair. Proc. Natl. Acad. Sci. USA 100, 4592–4597.

McNeil, P.L., Vogel, S.S., Miyake, K., and Terasaki, M. (2000). Patching plasma membrane disruptions with cytoplasmic membrane. J. Cell Sci. 113 (Pt. 11), 1891–1902.

Meaney, D.F., Smith, D.H., Shreiber, D.I., Bain, A.C., Miller, R.T., Ross, D.T., and Gennarelli, T.A. (1995). Biomechanical analysis of experimental diffuse axonal injury. J. Neurotrauma 12, 689–694.

Miyake, K., and McNeil, P.L. (1995). Vesicle accumulation and exocytosis at sites of plasma membrane disruption. J. Cell Biol. 131, 1737–1745.

Nehrt, A., Rodgers, R., Shapiro, S., Borgens, R., and Shi, R. (2007). The critical role of voltage-dependent calcium channel in axonal repair following mechanical trauma. Neuroscience 146, 1504–1512.

Povlishock, J.T., and Katz, D.I. (2005). Update of neuropathology and neurological recovery after traumatic brain injury. J. Head Trauma Rehabil. 20, 76–94.

Prado, G.R., Ross, J.D., DeWeerth, S.P., and LaPlaca, M.C. (2005). Mechanical trauma induces immediate changes in neuronal network activity. J. Neural Eng. 2, 148–158.

Raghupathi, R. (2004). Cell death mechanisms following traumatic brain injury. Brain Pathol. 14, 215–222.

Rami, A., Ferger, D., and Krieglstein, J. (1997). Blockade of calpain proteolytic activity rescues neurons from glutamate excitotoxicity. Neurosci. Res. 27, 93–97.

Saatman, K., Abai, B., Grosvenor, A., Vorwerk, C., Smith, D., and Meaney, D. (2003). Traumatic axonal injury results in biphasic calpain activation and retrograde transport impairment in mice. J. Cereb. Blood Flow Metab. 23, 34–42.

Saatman, K.E., Duhaime, A.C., Bullock, R., Maas, A.I., Valadka, A., and Manley, G.T. (2008). Classification of traumatic brain injury for targeted therapies. J. Neurotrauma 25, 719–738.

Sahay, K., Mehrotra, R., Sachdeva, U., and Banerji, A. (1992). Elastomechanical characterization of brain tissues. J. Biomechanics 25, 319–326.

Schlicher, R.K., Radhakrishna, H., Tolentino, T.P., Apkarian, R.P., Zarnitsyn, V., and Prausnitz, M.R. (2006). Mechanism of intracellular delivery by acoustic cavitation. Ultrasound Med. Biol. 32, 915–924.

Serbest, G., Burkhardt, M., Siman, R., Raghupathi, R., and Saatman, K. (2007). Temporal profiles of cytoskeletal protein loss following traumatic axonal injury in mice. Neurochem. Res. 32, 2006–2014.

Shi, R., Qiao, X., Emerson, N., and Malcom, A. (2001). Dimethylsulfoxide enhances CNS neuronal plasma membrane resealing after injury in low temperature or low calcium. J. Neurocytol. 30, 829–839.

Shi, R., and Whitebone, J. (2006). Conduction deficits and membrane disruption of spinal cord axons as a function of magnitude and rate of strain. J. Neurophysiol. 95, 3384–3390.

Singleton, R.H., and Povlishock, J.T. (2004). Identification and characterization of heterogeneous neuronal injury and death in regions of diffuse brain injury: evidence for multiple independent injury phenotypes. J. Neurosci. 24, 3543–3553.

Smith, D.H., Chen, X.H., Pierce, J.E., Wolf, J.A., Trojanowski, J.Q., Graham, D.I., and McIntosh, T.K. (1997). Progressive atrophy and neuron death for one year following brain trauma in the rat. J. Neurotrauma 14, 715–727.

Stein, S.C., Spettell, C., Young, G., and Ross, S.E. (1993). Delayed and progressive brain injury in closed-head trauma: radiological demonstration. Neurosurgery 32, 25–30; discussion 30–21.

Stone, J.R., Okonkwo, D.O., Dialo, A.O., Rubin, D.G., Mutlu, L.K., Povlishock, J.T., and Helm, G.A. (2004). Impaired axonal transport and altered axolemmal permeability occur in distinct populations of damaged axons following traumatic brain injury. Exp. Neurol. 190, 59–69.

Togo, T., Alderton, J.M., and Steinhardt, R.A. (2000). The mechanism of cell membrane repair. Zygote 8 Suppl. 1, S31–S32.

Villa, P.G., Henzel, W.J., Sensenbrenner, M., Henderson, C.E., and Pettmann, B. (1998). Calpain inhibitors, but not caspase inhibitors, prevent actin proteolysis and DNA fragmentation during apoptosis. J. Cell Sci. 111 (Pt. 6), 713–722.

Vosler, P., Brennan, C., and Chen, J. (2008). Calpain-mediated signaling mechanisms in neuronal injury and neurodegeneration. Molec. Neurobiol. 38, 78–100.

Weber, J.T. (2004). Calcium homeostasis following traumatic neuronal injury. Curr. Neurovasc. Res. 1, 151–171.

Weber, J.T., Rzigalinski, B.A., Willoughby, K.A., Moore, S.F., and Ellis, E.F. (1999). Alterations in calcium-mediated signal transduction after traumatic injury of cortical neurons. Cell Calcium 26, 289–299.

Whalen, M.J., Dalkara, T., You, Z., Qiu, J., Bermpohl, D., Mehta, N., Suter, B., Bhide, P.G., Lo, E.H., Ericsson, M., and Moskowitz, M.A. (2008). Acute plasmalemma permeability and protracted clearance of injured cells after controlled cortical impact in mice. J. Cereb. Blood Flow Metab. 28, 490–505.

Zhang, L., Rzigalinski, B.A., Ellis, E.F., and Satin, L.S. (1996). Reduction of voltage-dependent Mg2+ blockade of NMDA current in mechanically injured neurons. Science 274, 1921–1923.

Address correspondence to:
Michelle C. LaPlaca, M.D.
Georgia Institute of Technology/Emory University
Coulter Department of Biomedical Engineering
Petit Institute for Bioengineering & Bioscience
313 Ferst Drive
Atlanta, GA 30332-0535

E-mail: michelle.laplaca@bme.gatech.edu